https://doi.org/10.5194/essd-2026-63
Preprint. Discussion started: 4 February 2026

Open Access Earth System Science Data Discussions

Building a dataset of offshore oil and gas extraction platforms from satellite data (2017-2023)

Lulu Si [1], Shanyu Zhou [1], Itziar Irakulis-Loitxate [1,2], Javier Roger [1], and Luis Guanter [1,3]

[1]Research institute of Water and Environmental Engineering (IIAMA), Universitat Politècnica de València (UPV), 46022. Valencia, Spain.
[2]International Methane Emission Observatory (IMEO), United Nations Environment Programme, 75015. Paris, France.
[3]Environmental Defense Fund, Reguliersgracht 79, 1017 LN Amsterdam, The Netherlands.

Correspondence: Lulu Si (lsi@doctor.upv.es)

Abstract. Accurate information on the location and operational status of offshore oil and gas platforms (OOGPs) is important to inform decision-making by various stakeholders and to evaluate the environmental impacts of OOGPs. However, existing OOGP databases are often incomplete or outdated data. In this work, we use satellite data and the Google Earth Engine (GEE) platform to construct a new database of OOGPs for six major offshore oil and gas basins in the world between 2017 and 2023. We use synthetic aperture radar (SAR) images from the Sentinel-1 satellite mission to detect OOGP candidates due to its high sensitivity to OOGPs, dense spatio-temporal sampling, and global coverage. Our main processing steps comprise the detection of OOGP candidates using monthly averages of SAR images and the removal of noise and false positive objects from annual image composites. With the resulting dataset of OOGPs, we map the spatiotemporal distribution of OOGPs in the study regions and analyze platform status after the post-processing of the platform targets. Using these methods, we identified a total of 5,358 OOGPs distributed in six offshore basins: the Gulf of Mexico (GoM) (1,593), Persian Gulf (PG) (1,437), North Sea (440), Caspian Sea (CS) (794), Gulf of Guinea (460), and Gulf of Thailand (634). An independent validation dataset was used to evaluate the performance of the detection algorithm, which achieved an extraction accuracy of 98%. This OOGPs dataset substantially enhances and complements the existing offshore platform database in terms of spatial and temporal coverage. From our analysis of this OOGP dataset, we observed that offshore platform activity has declined in regions like the GoM due to infrastructure aging and policy shifts, while it has expanded in the PG and CS, reflecting ongoing offshore development. These different regional trends highlight the need for targeted environmental oversight and region-specific mitigation strategies.

1 Introduction

Offshore oil and gas platforms (OOGPs) serve as essential infrastructure for energy extraction and are widely used for drilling, extracting, and processing oil and natural gas, as well as for temporarily storing products before transporting them onshore for refining and sale (Tan et al., 2021). With advancements in offshore exploration technology and the depletion of onshore reserves, the continuous development and utilization of offshore oil and gas resources play an increasingly significant role in the global energy structure and economic development (Charfeddine and Barkat, 2020; Wang et al., 2023). According to the International Energy Agency (IEA) World Energy Outlook for 2024, two-thirds of the overall increase in energy demand in

https://doi.org/10.5194/essd-2026-63
Preprint. Discussion started: 4 February 2026

Open Access Earth System Science Data Discussions

2023 was met by fossil fuels, with oil and natural gas demand projected to peak by 2030 (IEA, 2024). OOGPs are widely distributed globally, with variations in design scale, complexity, and operational condition depending on platform type. Aging infrastructure nearing the end of its service life often faces challenges related to decommissioning due to structural degradation and escalating operational costs. These aging platforms typically have three potential decommissioning options: repurposing, recycling, and disposal, which may include full removal, partial dismantling, or conversion into artificial reefs or aquaculture facilities, respectively. However, both operational and decommissioned OOGPs pose environmental risks (Ekins et al., 2007; Cantle and Bernstein, 2015; Henrion et al., 2015; Irakulis-Loitxate et al., 2022), for example, when decommissioned offshore platforms are transported to land for dismantling and recycling, fossil fuel consumption can generate significant marine pollutants, posing serious threats to the ocean environment (Ronconi et al., 2015). Additionally, the removal of platforms, oil and gas processing equipment, and the dredging of accumulated shell mounds and debris beneath the structures can impact water quality (Bernstein, 2015). Moreover, greenhouse gas (GHG) emissions generated by fossil fuels will directly affect the achievement of the global carbon neutral and global warming targets (Alvarez et al., 2018; Nguyen et al., 2016; Allen et al., 2018; int, 2022). Growing concerns about the environmental and socioeconomic impacts of OOGPs have led to increased demand for effective monitoring (Lee, 2015; Anifowose et al., 2016; Hunt et al., 2022). Consequently, it is important to detect and monitor OOGPs to better understand their operational status and spatiotemporal patterns.

Despite the critical role of offshore infrastructure, publicly accessible and comprehensive datasets remain limited, especially beyond the Northern Gulf of Mexico (NGoM). This lack of data constrains our capability to assess offshore economies and their environmental impacts. While the Offshore Global Infrastructure Map (OGIM) offers an integrated geospatial perspective, its reliance on industry and regulatory data sources results in persistent gaps and delayed updates (Omara et al., 2023). Monitoring OOGPs is further hindered by their remote locations, harsh oceanic conditions, and high operational costs. Missteps can lead to severe consequences, including oil spills, gas leaks, and human injuries. These challenges underscore the need for advanced methods to determine the location and operational status of OOGPs. Remote sensing has emerged as a promising approach, offering large-scale, long-term, high-resolution, and continuous observational capabilities.

Remote sensing imagery provides rich spectral, textural, and temporal information, making it ideal for monitoring OOGPs. In recent years, a variety of remote sensing images have been used to monitor activities on the sea surface (Spanier and Kuenzer, 2024). The high reflectance characteristics of the metal-concrete structures, along with the high-temperature exhaust gases of OOGPs in the visible and near-infrared bands, enable their automatic extraction in nighttime imagery (Casadio et al., 2012; Elvidge et al., 2016a; Zhao et al., 2017). Time-series of optical imagery have also been used for the detection of offshore platforms (Liu et al., 2016; Zhu et al., 2021). However, widely used passive optical sensors are limited by weather conditions (e.g., clouds and fog), which hinder consistent monitoring. To overcome these limitations, synthetic aperture radar (SAR) represents a promising alternative for extracting OOGPs because it can easily penetrate clouds and detect metallic objects on the sea surface with complex backgrounds (Peng et al., 2011; Casadio et al., 2012; Jiasheng et al., 2013; Falqueto et al., 2019; Wong et al., 2019). Dual-polarization SAR, such as that provided by Sentinel-1, has a stronger ability to distinguish the details of the facility structure, which enables facilitates detection more accurate. Nonetheless, existing algorithms based on Sentinel-

https://doi.org/10.5194/essd-2026-63
Preprint. Discussion started: 4 February 2026

1 SAR data are prone to false positives, especially in complex oceanic surface conditions, limiting large-scale and accurate extraction of OOGPs.

In this study, we developed a automated and robust framework for systematically extracting OOGPs and unveiling their spatial distribution patterns from 2017 to 2023. The key contributions of this study include (1) the development of a high-accuracy algorithm tailored to Sentinel-1 SAR imagery for detecting OOGPs, and (2) the construction of a comprehensive and openly available spatiotemporal dataset that enables in-depth analysis of OOGP development from 2017 to 2023.

2 Materials

2.1 Study area

The selection of Regions of Interest (ROI) was primarily based on their relevance to OOGP activities. This study focused on six offshore regions with known high concentrations of OOGP activity according to the OGIM database: the Gulf of Mexico (GoM), Gulf of Thailand (GoT), Caspian Sea (CS), Gulf of Guinea (GoG), Persian Gulf (PG), and North Sea (NS). These areas are globally significant centers of offshore energy production, representing major hubs of offshore industrial infrastructure.

In five of the six selected regions (GoM, GoT, GoG, PG, and CS), a number of offshore methane plumes were detected between 2021 and 2025 based on data from the United Nations Environment Programme (UNEP)'s Methane Alert and Response System (MARS) (https://methanedata.unep.org/) and the Carbon Mapper initiative (https://data.carbonmapper.org/) (See Fig. 1). These detections indicate the presence of methane emissions likely associated with intensive OOGP activities. While methane plume detection efforts are not globally uniform, the data broadly reinforce the relevance of the chosen regions for emission monitoring and analysis. Although no offshore methane plumes were reported in the NS during this period, it is characterized by a high density of oil and gas platforms, as well as a key site for offshore wind infrastructure (Hoeser et al., 2022). Its inclusion highlights the broader relevance of offshore infrastructure for emission monitoring and mitigation strategies.

Together, the inclusion of all six regions ensures comprehensive spatial coverage of major offshore energy hubs and provides a robust foundation for evaluating current methane emissions, offshore infrastructure patterns, and emerging energy transitions.

OOGPs in upstream operations in offshore areas serve as key facilities for the exploration, production, storage, and transportation of oil and gas resources. To better understand the spatial and functional complexity of these installations, it is essential to recognize the diversity of OOGP types deployed in various marine environments. This diversity reflects varying engineering strategies, water depths, and operational requirements across regions. Figure 2 illustrates representative examples of major oil and gas production infrastructure types, highlighting their structural and functional diversity observed in the selected study areas. Understanding the configuration and distribution of these platform types provides an important context for interpreting satellite-detected infrastructure patterns and assessing their environmental footprints. This foundational overview sets the stage for the following sections, which detail the methods used to extract, classify, and analyze OOGPs using satellite data.

https://doi.org/10.5194/essd-2026-63
Preprint. Discussion started: 4 February 2026

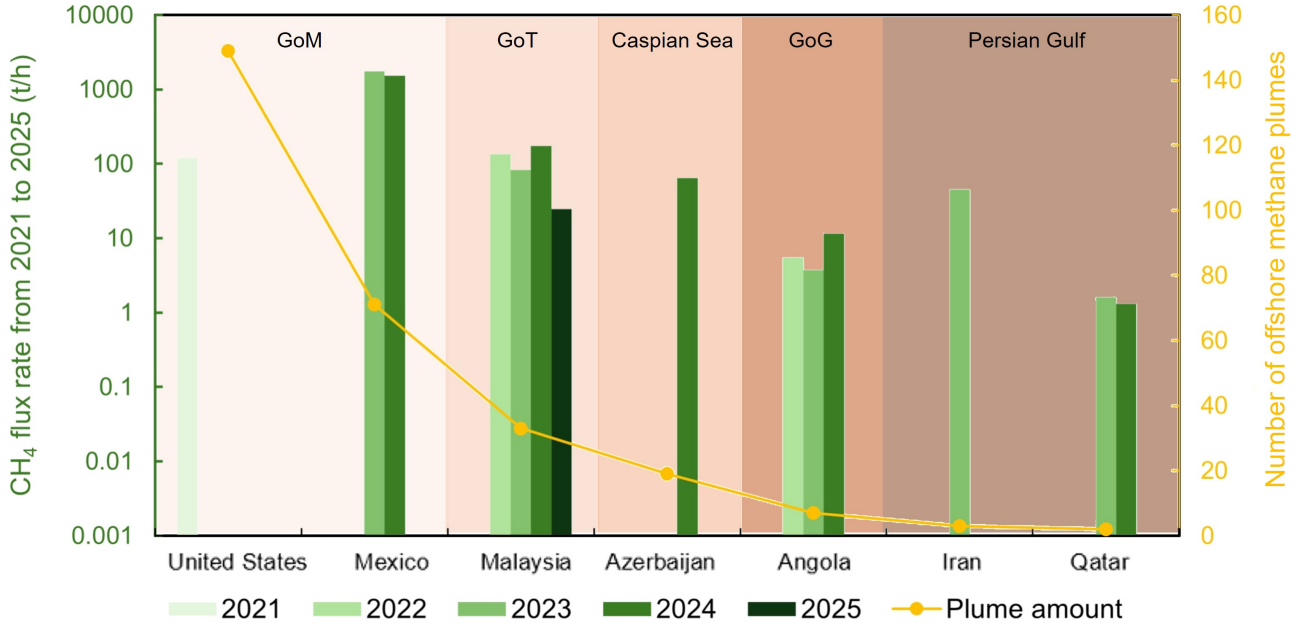

Figure 1. Global temporal variation of the total CH_4 flux rates from all the emissions and offshore methane plume amount generated by OOGPs in the leading nations from 2021 to 2025

2.2 Satellite data

The Sentinel-1 mission, part of the Copernicus Joint Initiative of the European Commission (EC) and the European Space Agency (ESA), provides dual-polarization C-band SAR data operating at 5.405 GHz. Data are delivered as Level 1 Ground Range Detected (GRD) scenes containing calibrated backscatter coefficients (σ°) expressed in decibels (dB), with spatial resolutions of 10, 25, or 40 m depending on the acquisition mode. The available polarization configurations include single-polarization modes as Vertical transmit/Vertical receive (VV) and Horizontal transmit/Horizontal receive (HH), as well as dual-polarization modes like Vertical transmit/Horizontal receive (VV + VH) and Horizontal transmit/Vertical receive (HH + HV). In this study, Sentinel-1 SAR images were collected and processed using the GEE platform through 'COPERNICUS/S1_GRD' image collection, which consists of GRD scenes from 2014 onward. GEE applies automated preprocessing workflow that includes thermal noise removal, radiometric calibration, and terrain correction using either the SRTM 30 m DEM or ASTER GDEM for latitudes above 60°, where SRTM data is unavailable. This ensures the production of consistent, analysis-ready SAR imagery suitable for large-scale time series analysis.

Sentinel-1's C-band SAR operates independently of all-weather, day-and-night capability, making it well-suited for continuous observation of offshore environments and detecting changes over time. For OOGPs detection, we used Sentinel-1 imagery

https://doi.org/10.5194/essd-2026-63
Preprint. Discussion started: 4 February 2026

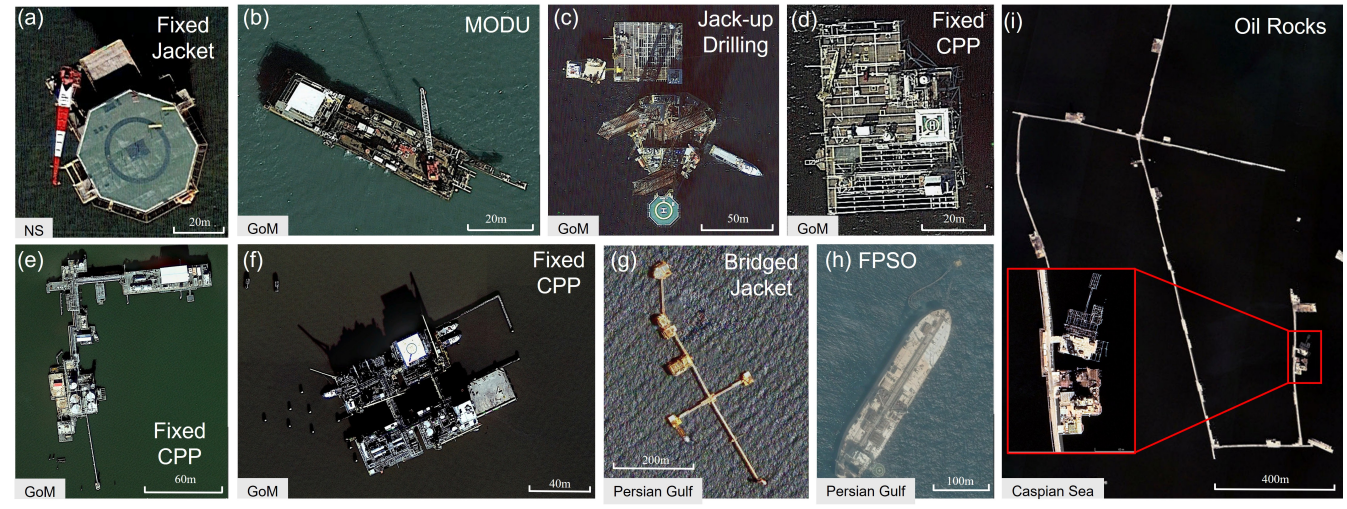

Figure 2. High resolution images showing major OOGP types (© Google Earth). (a) Single fixed jacket platform. (b) Moveable Offshore Drilling Unit (MODU) with drilling tower. (c)Jackup Drilling Platforms/Rigs with helideck, hull, leg and apudcan. (d) Central Processing Platform (CPP). (e) Rectangular-shaped bridged fixed production platform with storage tanks and pipelines. (f) Bridged integrated production platform with well, mooring buoys (white points), vent flare boom, distillation/absorption tower, tanks, piplines, oil and gas seperation, helipad and transport vessels. (g) Bridged fixed jacket platform with flaring on South Pars natural gas field. (h) Floating production, storage and offloading (FPSO) vessels on South Pars natural gas field. (i) Oil rocks combined with residential infrastructure and long interconnected metal causeways in Caspian Sea. (a) Located in the NS. (b-f) Located in GoM, USA. (g-h) Located in the Persain Gulf. (i) Located in Caspian Sea, Azerbaijan.

in VH polarization from 2017 to 2023. VH-polarized backscatter is particularly sensitive to complex metallic structures with depolarizing properties, such as cranes, pipelines, helipads, and OOGPs, which typically involve vertical and horizontal components. These structures induce cross-polarized signals through multiple scattering, corner reflections, and geometric complexity, making VH band images an effective choice for OOGP detection. Conversely, to exclude Offshore Wind Turbines (OWTs), we utilized imagery acquired in Interferometric Wide (IW) swath mode and VV polarization. OWTs, usually composed of tall, smooth metallic towers with rotating blades, produce strong and stable VV backscatter as their regular geometry and high reflectivity. This makes VV polarization effective for masking OWTs during OOGPs mapping.

To support the detection of offshore gas flaring (GF) activities, we incorporated Sentinel-2 imagery as a complementary data source. GF refers to the combustion of excess or unusable gases released during oil and gas extraction, typically through flare stacks at production facilities (Elvidge et al., 2015). These flaring activities are often characterized by high-temperature signatures that can be captured in the shortwave infrared (SWIR) bands of Sentinel-2 imagery (Faruolo et al., 2023). Sentinel-2, launched by the European Space Agency (ESA) under the Copernicus program, provides high-resolution multispectral imagery with frequent global coverage. Its SWIR bands are particularly useful for identifying thermal anomalies, making it suitable for

https://doi.org/10.5194/essd-2026-63
Preprint. Discussion started: 4 February 2026

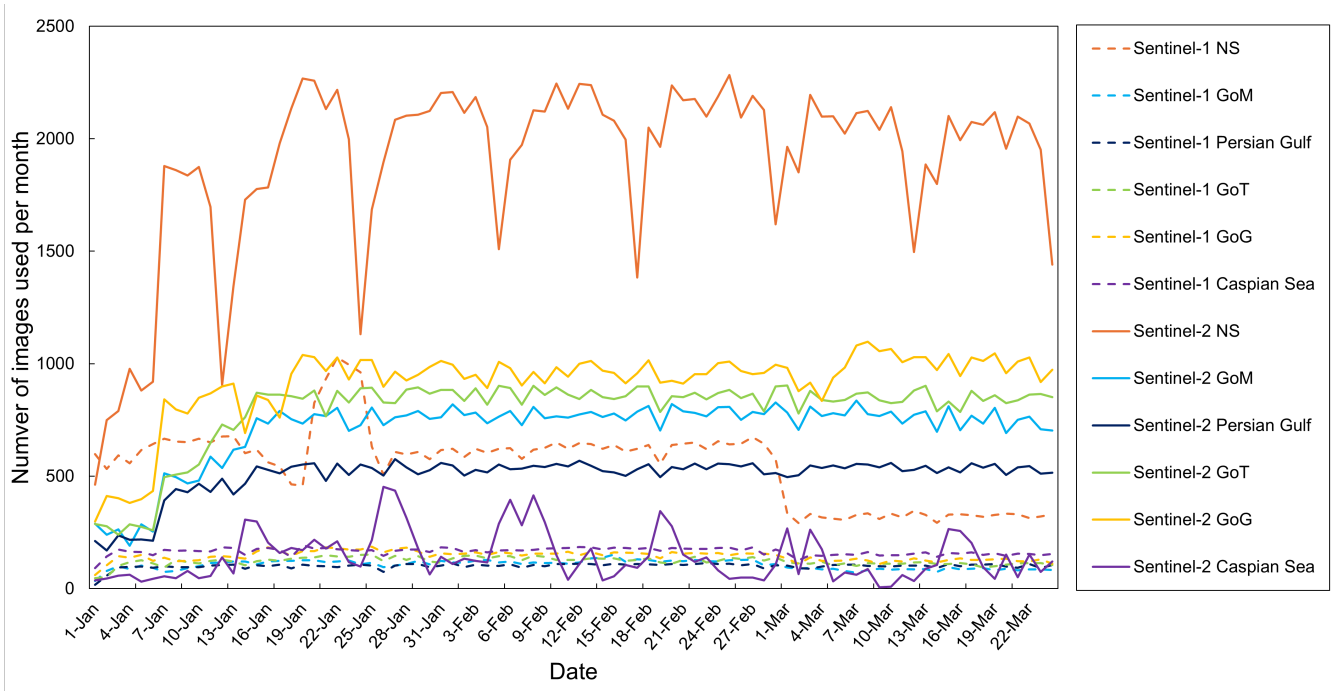

Figure 3. Statistics of the number of Sentinel-1 and Sentinel-2 images used in this study.

detecting and validating offshore GF events in high resolution. The imagery used in this study was obtained from the GEE platform ('COPERNICUS/S2_HARMONIZED'), covering the period from 2017 to the present.

The main geometric and spectral characteristics of each sensor are summarized in Table 1. A total of 99,784 Sentinel-1 images were used for the OOGPs detection algorithm and time series analysis, and 416,070 Sentinel-2 MSI images were used for locating and monitoring GFs. The number used per month is shown in Fig. 3.

Table 1. Nominal parameters of optical passive and SAR active sensors whose data were used in this study.

Sensor	Acquisition mode	Swath (km)	Spec. range	Band no.	Temporal res. (day)	Spatial res. (m)
Sentinel-1 SAR	IW	250	C-band SAR (5.405 GHz)	1	6	5x20
Sentinel-2 MSI	Push-broom scanning	290	0.4-2.2 um	13	5	10/20/60

2.3 Auxiliary data

2.3.1 Maritime zoning

To contextualize offshore platform distribution by national jurisdiction, we used the Exclusive Economic Zones (EEZs) database, which defines maritime boundaries established by the 1982 United Nations Convention on the Law of the Sea.

https://doi.org/10.5194/essd-2026-63
Preprint. Discussion started: 4 February 2026

Within these boundaries, a sovereign nation has exclusive rights to explore and utilize marine resources. The EEZ data used in this study were obtained from the Open Data Platform Marine Regions (https://www.marineregions.org/eezsearch.php), which provides EEZ boundaries for all countries. This dataset was used to explain the geographical features of OOGPs within the EEZ of each country.

2.3.2 Validation datasets

We utilized four primary geospatial platform datasets to validate the OOGP detection results, as described in Table S1 in the Supplementary Material. A detailed description of each dataset is provided below.

The Bureau of Safety and Environmental Enforcement (BSEE) provides offshore platform information on the federal waters of the NGoM (from the boundary of state waters to 200 nautical miles), including detailed attributes such as structure type, installation and removal dates, operational status, and production flags. The latest BSEE release contains 7,303 records describing both existing and removed platforms (https://www.data.bsee.gov/). However, BSEE does not cover platforms located within state jurisdictions. To complement this limitation, we also used the NOAA Offshore Oil and Gas Platforms dataset (https://hub.marinecadastre.gov/datasets/noaa::offshore-oil-and-gas-platforms/about), which provides point locations of platforms in both state and federal waters. NOAA's product with broader spatial coverage makes it a robust supplementary dataset for validating satellite-derived detections in the NGoM.

For the NS, we used the Offshore Energy Structures in the North Sea (later on, referred to as OESNS) dataset from the University of St Andrews as the primary validation source (Martins et al., 2023). To assist in identifying and removing false positives, we also used vessel traffic management zones from the UK Hydrographic Office (https://datahub.admiralty.co.uk/portal/home/index.html, which delineate major shipping corridors.

The global geospatial database named OGIM also provides information on major global oil and gas facilities, including type, location, operational status, operators' name in some countries, and installation dates (Omara et al., 2023). Overall, these dataset was acquired, curated, and integrated from public domain geospatial datasets reported by official government sources, industries, academic research institutions, and other non-governmental entities. It is limited by the open-access availability of geospatial datasets and cannot efficiently obtain spatiotemporal continuity changes in real time.

Among the total records of existing platforms, some structures belonging to the same platform were recorded individually in the first three platform database (Fig.S1). Thus, we determined the actual counts of existing platforms through the unique identifiers. This process eliminated redundant data and ensured the accuracy of the validation data.

Together, these databases provide reliable references for validating OOGP detections. Moreover, the detection results of this study will supplement the previously mentioned data records.

To further verify platform activity status and cross-reference with our OOGPs detections, we incorporated active fire data distributed by the Fire Information for Resource Management System (FIRMS : https://firms.modaps.eosdis.nasa.gov/) (Elvidge et al., 2016b, a) and dense ship regulated area provided by UK Hydrographic Office (https://www.admiralty.co.uk/access-data/marine-data in this study. Detected hot spots in the FIRMS portal within proximity to known OOGPs locations are interpreted as active GF events. By overlaying fire points and dense ship lane polygons onto satellite-detected platform locations, these

https://doi.org/10.5194/essd-2026-63
Preprint. Discussion started: 4 February 2026

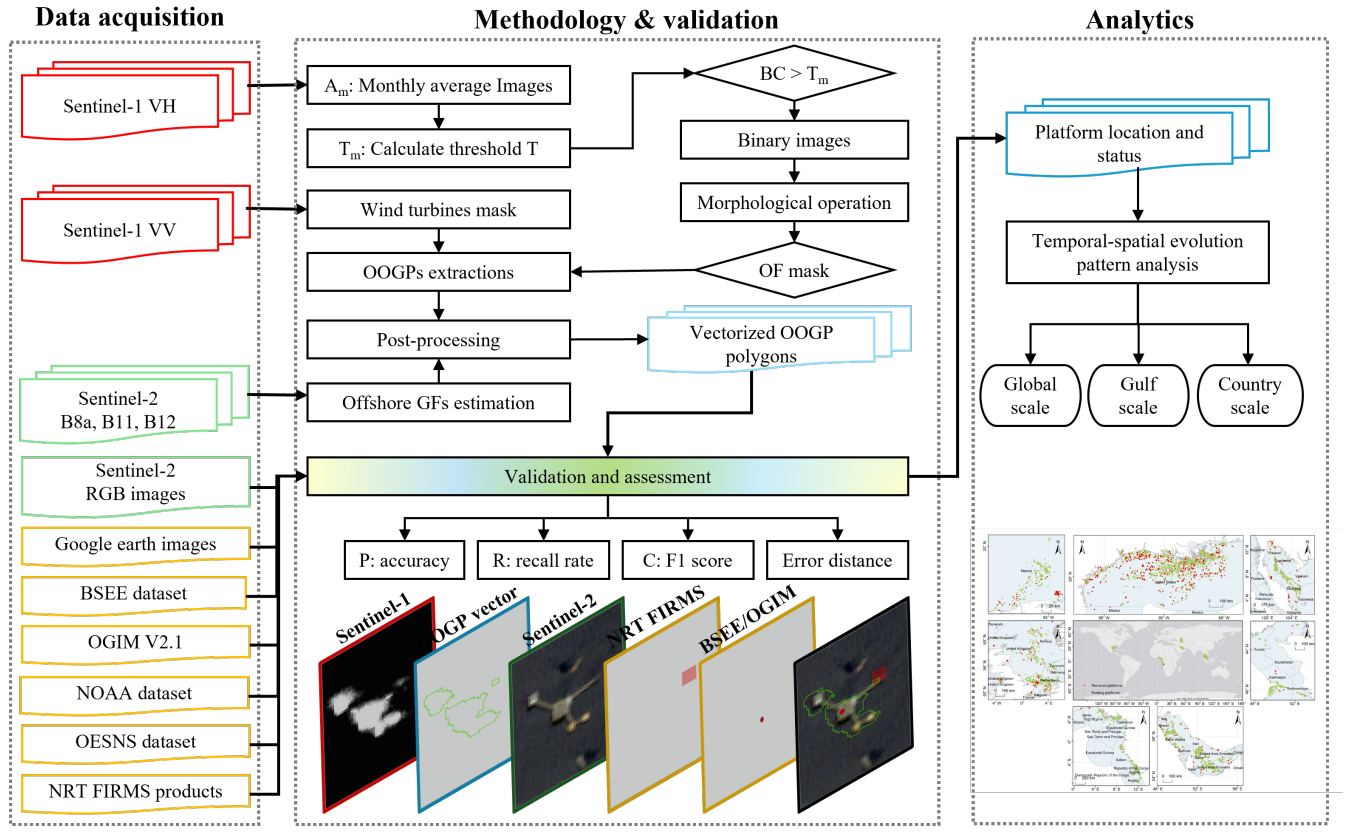

Figure 4. Framework of the study used to develop OOGPs data set. OF:Occurance Frequency, BC:Backscattering Coefficients. See text for acronyms.

auxiliary datasets ensure the accuracy of platform identification and distinguish operational platforms from other structures or false positives. The temporal and spatial consistency between the FIRMS fire product and primary satellite datasets further enhances the robustness of platform detection and analysis.

3 Methodology

The OOGPs dataset was developed using geospatial analysis with Sentinel-1 SAR and Sentinel-2 time-series imagery on the GEE platform and Python-based workflows. The detailed framework is presented in Fig. 4. It mainly includes: (1) detecting platforms based on monthly averages of Sentinel-1 images; (2) removing noise and false positive objects from long time-series images; and (3) mapping platform spatial distribution and analyzing platform status after the post-processing of the platform targets.

https://doi.org/10.5194/essd-2026-63
Preprint. Discussion started: 4 February 2026

Open Access Earth System Science Data Discussions

3.1 Processing of Sentinel-1 data

In this study, we selected Sentinel-1 imagery from the IW swath mode and VH polarization for the initial inspection of the platforms. As described in Section 2.2, this configuration was selected because it is more effective in detecting OOGPs than others. As shown in Fig. 5, we compared the backscatter coefficients of the Sentinel-1 VH polarization band of the subset area of the ROI. The backscattering coefficients in the VH band of Sentinel-1 effectively distinguish offshore platforms from open water. Specifically, if the maximum backscatter coefficient of a pixel (BC_{max}) from one monthly average image is less than -20, no platform facilities are present in that area. Therefore, the initial inspection of OOGPs in this study was performed based on the following criteria.

$$\text{Pixel (include or not)} = \begin{cases} \text{exclude}, & BC_{\text{max}} < -20\,(\text{dB}) \\ \text{include}, & \text{otherwise} \end{cases} \tag{1}$$

3.2 OOGPs candidates detection

Selecting an appropriate detection threshold for monthly averages of Sentinel-1 VH images is a critical step in initially identifying candidate targets. In regions with existing platforms, radar backscatter coefficients tend to be significantly higher than in surrounding open waters. This difference is reflected in the backscatter intensity curves in Fig. 5, where non-platform areas show peak at lower values. Considering regional variability in sea surface backscatter, we applied an adaptive threshold strategy. For each month (m), the adaptive threshold (T_m) was set to the 90th percentile of each monthly averages backscatter intensity (A_m) within ROIs and used to classify pixels into potential target areas as binary images. Here, the choice of the 90th percentile was informed by threshold sensitivity experiments, as shown in Table S2 and Fig.S2 in the supplementary material, which evaluated detection performance using three percentile levels (85th, 90th, and 95th). Lower thresholds lead to increased sea surface noise, whereas higher thresholds miss small or weakly reflective platforms. The 90th percentile provides the most balanced trade-off between completeness and the suppression of noise-induced artifacts. Although this inclusive threshold may retain some transient objects, they are subsequently removed through the temporal persistence filtering procedure described in Section 3.3.1. This percentile-based thresholding ensures the robust and regionally consistent detection of OOGPs under varying marine conditions. The detailed rules are as follows:

$$B_m = \begin{cases} 1, & A_m > T_m \\ 0, & A_m \leq T_m \end{cases} \tag{2}$$

$$A_m = \frac{1}{n}\sum_{i=1}^{n} BC_{i,m} \tag{3}$$

https://doi.org/10.5194/essd-2026-63
Preprint. Discussion started: 4 February 2026

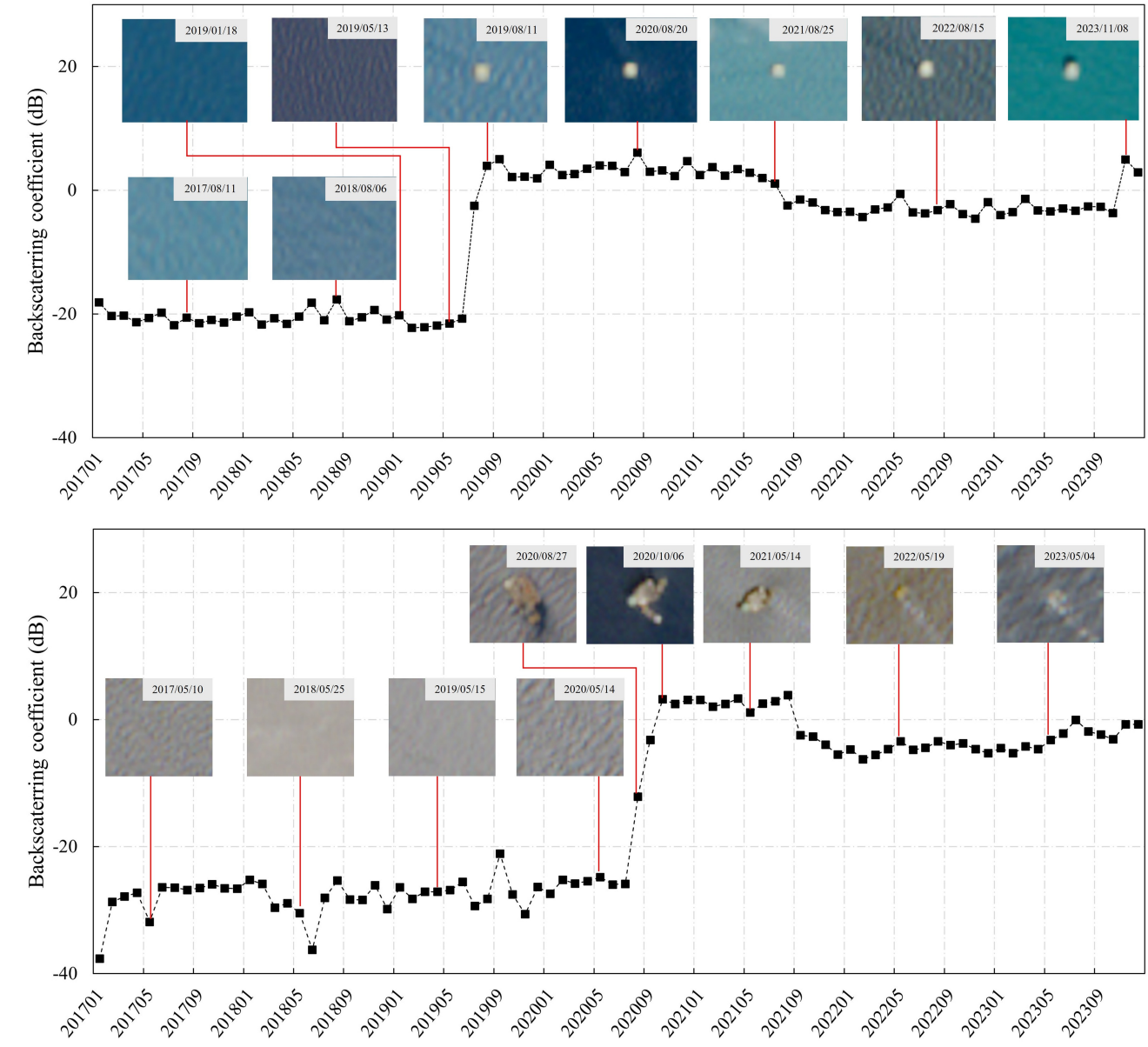

Figure 5. VH backscattering coefficient variation curves of the examples OOGPs from 2017 to 2023 and Sentinel-2 MSI true color images cover the example region. (a) Example OOGP in the GoM (92.18° W, 19.07° N). (b) Example OOGP in the Persian Gulf (52.02° E, 26.44° N).

$$T_m = 0.9 \times A_m, \quad m = 1, 2, \ldots, 12 \tag{4}$$

https://doi.org/10.5194/essd-2026-63
Preprint. Discussion started: 4 February 2026

Where $B_m$is the monthly binary image, T_m is the dynamic threshold of every monthly Sentinel-1 VH image, BC_m is the backscatter coefficient of each pixel in the single monthly average image, and n is the number of Sentinel-1 images every month.

3.3 OOGPs refinement and post-processing

OOGPs refinement and post-processing were performed systematically by applying following three steps: (1) Removal of noise and mobile objects. (2) Removal of OWTs. (3) Post-processing of platforms dataset. A detailed explanation of each section follows.

3.3.1 Removal of noise and mobile objects

The binary images produced with the methods described in Section 3.2 may be distorted by noise and texture, and some islands or small objects may be present. These false objective targets often have spatiotemporal discontinuities and are small in size. A morphological operation was applied to the binary images to eliminate interference and improve the accuracy of target detection. This operation employed eight-connected component analysis and an opening operation on the binary image. Specifically, the morphological opening operation refers to erosion processing in a 3×3 window, which replaces each pixel with the minimum value of its neighborhood to remove isolated islands and small noise points. Dilation processing assigns each pixel with the maximum value in its 3×3 neighborhood to restore the original target area boundary and fill holes caused by erosion. After spatial noise reduction through morphological processing, advanced statistical analysis based on the Occurrence Frequency (OF) of the VH signal was performed to remove floating or temporarily moving objects (e.g., ships and sun glints) using Sentinel-1 monthly averages per year. Platforms, which are stationary infrastructures, maintain stable radar backscatter and thus exhibit high OF values. In contrast, mobile objects such as ships appear only intermittently and therefore display a low OF (Fig.S3). To account for different sea states and shipping intensities, we applied region-specific OF thresholds determined through sensitivity testing and manual inspection: OF $\geq$ 2 in the GoG and GoT; OF $\geq$ 3 in the GoM, inner PG and CS; OF $\geq$ 6 in the open-water North Sea and nearshore PG; and OF = 12 in the heavily trafficked English Channel. Based on this processing, false-positive targets caused by sea surface conditions, such as ocean clutter and frequent passing ships, were eliminated, and the resulting vector polygons were used for the platform's post-processing.

3.3.2 Removal of offshore wind turbines

Offshore wind farms (OWFs), consisting of OWTs, are widely distributed in the vicinity of oil and gas production facilities in offshore economic zones, mainly in the NS and coastal areas of China. Their local spatiotemporal distribution characteristics are similar to those of OOGPs, making them typical false-positive targets. Owing to the increasing expansion of OWFs at existing and recently developed wind energy production sites, a holistic understanding and detailed insights into their distribution are gaining importance for obtaining accurate OOGP locations. Considering that the VV polarization band is more effective in detecting OWFs, this study used Sentinel-1 imagery in IW swath mode and VV polarization to improve detection accuracy. A

https://doi.org/10.5194/essd-2026-63
Preprint. Discussion started: 4 February 2026

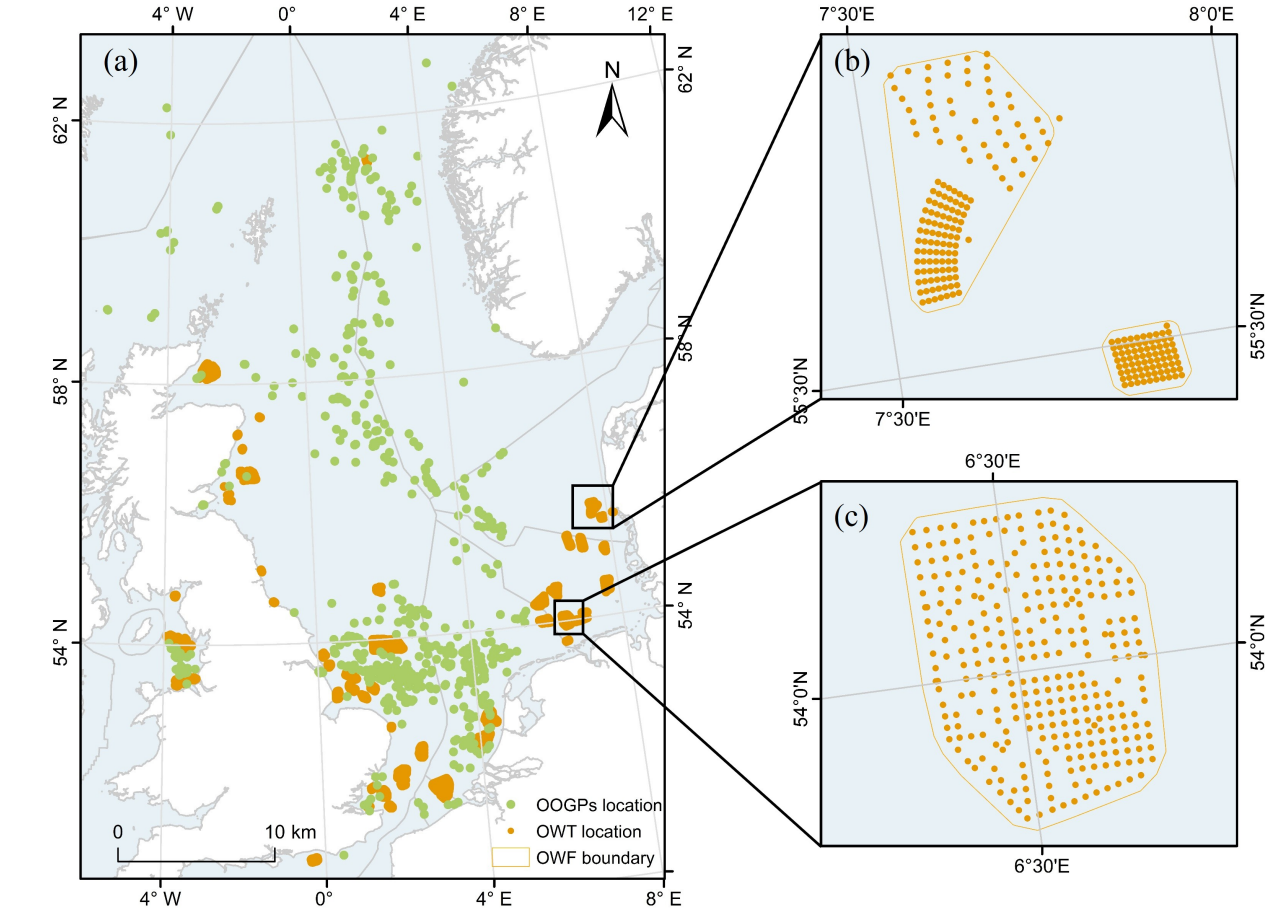

Figure 6. Detection results of OWTs in NS. (a) Points of OOGPs detected using Sentinel-1 VH images and OWTs identified from Sentinel-1 VV imagery in NS. (b-c) Selected examples of OWTs within the OWF boundaries in NS. All data were collected from 2017 to 2023.

percentile-based yearly image reduction method, combined with an auto-adaptive threshold algorithm on the GEE platform, was applied to suppress false positives and better isolate OOGP targets (Fig.S4) (Zhang et al., 2021). We detected 5481 OWTs within 53 OWFs in NS from 2017 to 2023. The OWTs dataset will also be open access and distributed along with our OOGPs dataset as ancillary information. Figure 6 provides an overview of all detected objects and their boundaries throughout the entire time series in the OOGPs dataset, from which our OWTs detection contributes to distinguishing OOGPs from widespread wind energy infrastructures. See procedure details of OWTs detection in appendix.

https://doi.org/10.5194/essd-2026-63
Preprint. Discussion started: 4 February 2026

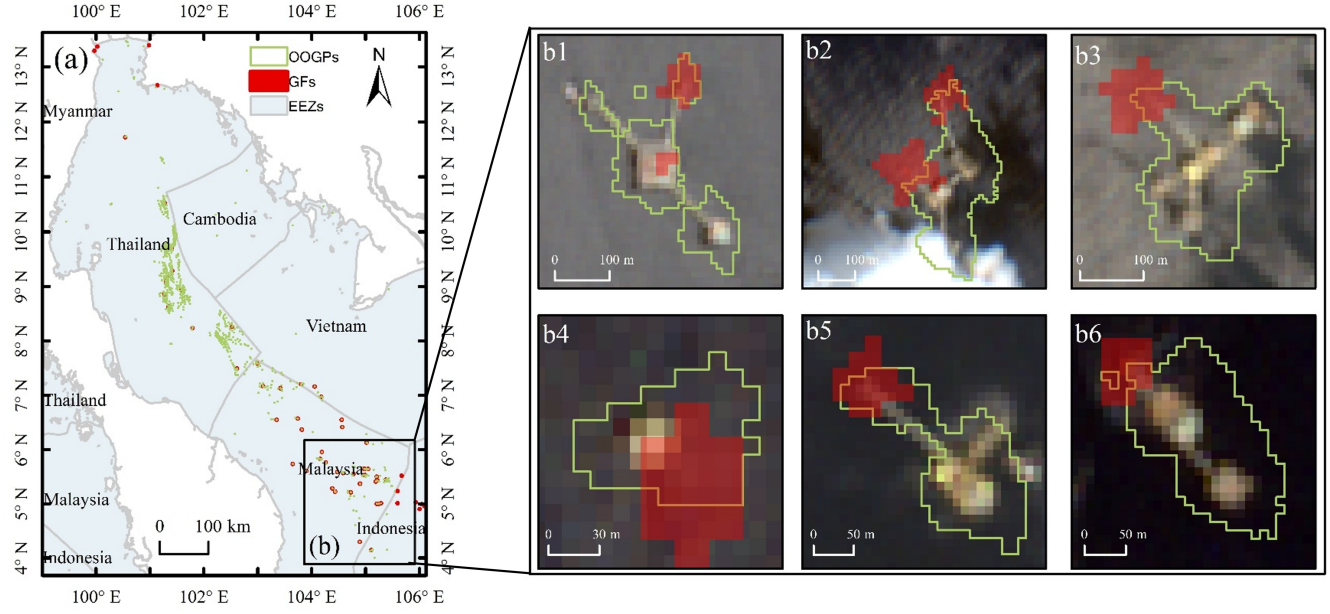

Figure 7. Detection of GFs in the GoT. (a) Boundaries of OOGPs detected using Sentinel-1 VH images and GFs identified from Sentinel-2 imagery within different EEZs in the GoT. (b1–b6) Selected examples of GFs produced by OOGPs. Red areas represent gas flaring (GF) signals derived from Sentinel-2 SWIR bands. Green polygons indicate the outlines of offshore oil and gas platforms (OOGPs) detected by Sentinel-1. Sentinel-2 RGB images were used as the basemap. All data are from 2023.

3.3.3 Postprocessing of platforms dataset

To estimate the detailed status of OOGPs, we need to further determine the location, installation date, EEZ, and GF flag for each OOGP. Here, we converted the raster data without false positive targets and noise into a vector polygon layer and calculated the centroid to obtain the location of each platform.

As to the indicator of whether there is approved burning or disposition of produced gas through a single OOGP (Fig. 7), we adopted the Thermal Anomaly Index (TAI) method to detect High-Temperature Anomalies (HTA) from single-phase Sentinel-2 MSI Top-Of-Atmosphere (TOA) reflectance images, and then refined offshore GF site candidates among the time-series detections (Liu et al., 2023).

As shown before in Fig. 5, the backscatter coefficient increased substantially after the construction of the platform. To further determine the status and construction time of the platform facilities, we used long time-series SAR data to identify annual drastic change points using the Mann-Kendall (MK) method (Mann, 1945; Kendall, 1948; Hamed, 2008). The MK test is a non-parametric statistical test that determines the trend direction by comparing the relationships between all data points in continuous time series. We created a candidate zone on the platform facility and extracted the monthly maximum backscatter coefficient from this buffer as the input value for the MK test. The operation was performed using GEE and MATLAB.

https://doi.org/10.5194/essd-2026-63
Preprint. Discussion started: 4 February 2026

Table 2. Attributes and descriptions of the OOGP dataset

Attribute	Data Type	Description
Latitude	Float	Latitude of the OOGP centroid
Longitude	Float	Longitude of the OOGP centroid
Area	Float	Footprint area of the OOGP (km^2)
Country	String	Country where the OOGP is located
EEZ	String	EEZ where the OOGP is located
Installation date	Integer	Date when the OOGP was installed (yyyymm)
Removal date	Integer	Date when the OOGP was removed (yyyymm)
Flaring status	Integer (0/1)	Indicator of flaring activity (1 = flaring)

It is important to note that some platforms have a long lifespan and early installation time, but Sentinel-1 imagery (starting in 2014) is not sufficient to fully cover the installation time of all platforms, which introduces an incomplete capture of the actual installation date. Despite the partial biases, the MK method and long-term Sentinel-1 data are still reliable choices for detecting the installation date of OOGPs by signal variation. In this study, the statistical values with a significant trend of time series were selected by setting serial values with Z-value greater than 0.05 of the MK statistic of long time series backscatter coefficient. Two representative sites were chosen for a detailed visual assessment of the OOGP installation dates on a monthly scale. Finally, using auxiliary data, spatial analysis was conducted to compile attribute tables for each platform to obtain complete status information. Description of attributes are tabulated in Table 2.

3.4 Validation and uncertainty analysis

OOGPs detection is subject to uncertainty due to a variety of background factors, including sun glint, water turbidity, wind farms, and temporary moving objects. However, there is currently no set of consistent OOGPs to verify the precision and accuracy of this algorithm. To comprehensively assess the performance of our OOGPs dataset, we collected and generated a validation dataset in our study areas to quantify the accuracy metrics. Validation data include: (1) comparisons across multiple source datasets, including the BSEE and OGIM databases; (2) high-resolution imagery and Google satellite images for comprehensive visual interpretation and extensive internal review; and (3) time-series VIIRS fire products.

Because the latest available OGIM data records for 2023 are limited, the OGIM data for 2022 and BSEE data for 2023 were filtered for comparative analysis. Subsequently, we evaluated the performance of the proposed framework in detecting OOGPs from 2017 to 2023 using an independent accuracy assessment approach at the facility and regional levels.

We used the spatial analysis tools of ArcGIS software to match the locations of the detected OOGPs with reference datasets and evaluate their spatial positioning errors. The spatial deviation between the detected platforms and reference data was quantified by calculating the mean, standard deviation, median, maximum, and minimum values of the distance errors between matched points.

https://doi.org/10.5194/essd-2026-63
Preprint. Discussion started: 4 February 2026

In addition, the robustness of the detection method was investigated by calculating the accuracy P, recall rate R, and F1-score, the harmonic mean of precision and recall that balances the trade-off between the two metrics. These metrics are defined as follows:

$$P = \frac{TP}{TP + FP} \tag{5}$$

$$R = \frac{TP}{TP + FN} \tag{6}$$

$$F1\text{-}score = \frac{2 \times P \times R}{P + R} \tag{7}$$

where TP is the number of accurately identified offshore platforms, FP is the number of falsely identified offshore platforms, and FN is the number of offshore platforms omitted.

4 Results and discussion

4.1 Assessment of OOGP detection results

4.1.1 Detection accuracy assessment and comprehensive visual interpretation

A total of 3934 sample points covering six offshore regions were selected for validation in 2023. The validation was conducted using a combination of authoritative databases and visual interpretation, based on validation datasets composed of NOAA-BSEE, OGIM, OESNS, FIRMS, Sentinel-2 MSI imagery, and Google Earth high-resolution images. Specifically: In the federal waters of NGoM (US), 1349 OOGPs were validated using the NOAA and BSEE database with detailed information on platform location and structure type. In the Southern Gulf of Mexico (SGoM), 195 OOGPs were cross-validated by visual inspection using Sentinel-2 MSI imagery and Google Earth. For the PG, GoT, GoG, NS, and CS, a combined total of 2585 OOGPs were verified through multi-source visual inspection using Sentinel-2 MSI imagery, OGIM and OESNS records, FIRMS data, and high-resolution Google Earth images. The evaluation results are reported in Table 3. Precision scores for identified platforms reached 100% in the CS and GoG, 99% in the NS and PG, 97% in the GoM, and 96% in the GoT. Minor false positives were primarily associated with coastal structures such as antennas, fishing facilities, and historical landmarks with similar spatial signatures, as illustrated in Fig. 8. Recall scores, representing detection completeness, reached 99% in the NS, GoG and CS, followed by 96% in the GoT. Lower recall was observed in the GoM (84%), largely due to small-scale wellhead platforms below Sentinel-1's detection threshold. The F1 scores (harmonic mean of precision and recall) indicate the highest performance in the GoG and CS (100%), followed by the NS (99%).

Overall, the detection framework demonstrates robust accuracy and completeness across diverse offshore regions. Our results offer high accuracy in both spatial precision and temporal consistency, effectively complementing existing data products.

https://doi.org/10.5194/essd-2026-63
Preprint. Discussion started: 4 February 2026

Open Access Earth System Science Data Discussions

Table 3. Overview of all validation matrics for the OOGPs detections using Sentinel-1 imagery in 2023.

Region	Number of Samples	TP	FP	FN	P	R	F1
PG	400	367	3	33	0.99	0.92	0.95
CS	830	827	0	3	1.00	0.99	1.00
GoM	1886	1544	46	296	0.97	0.84	0.90
GoG	427	423	0	4	1.00	0.99	1.00
GoT	100	96	4	4	0.96	0.96	0.96
NS	443	436	4	3	0.99	0.99	0.99
Total	3934	3713	57	343	0.98	0.92	0.95

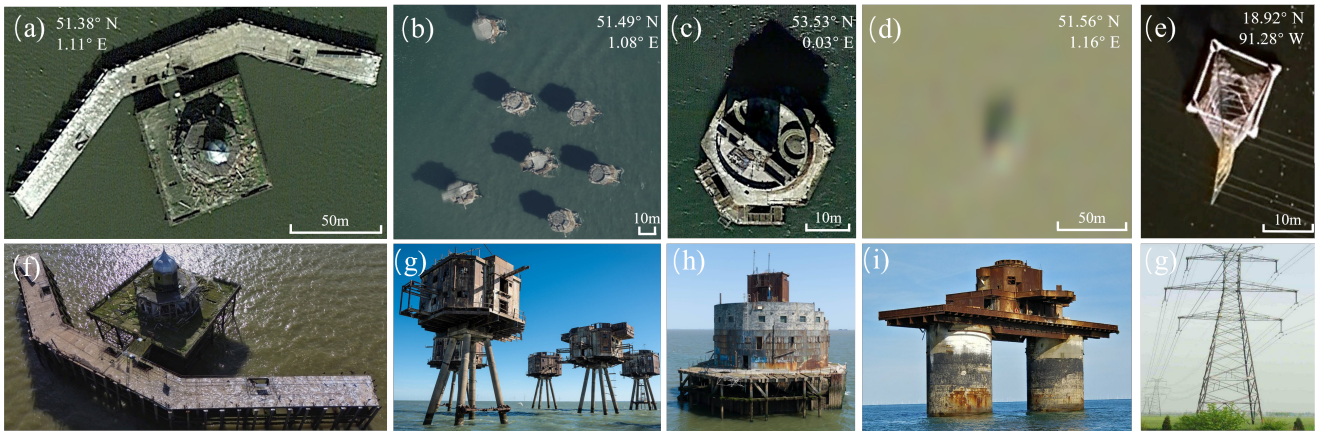

Figure 8. Examples of false positive targets in high-resolution imagery (© Google Earth). (a, f) Old pier structure with dome and extented corridors, located in Herne Bay, England. (b, g) A cluster of seven towers known as the Shivering Sands Army Fort, located offshore from Herne Bay, England. (c, h) Hexagonal Haile Sand Fort made of armored concrete, located off the coast of Cleethorpes, England. (d, i) Knock John Fort made of concrete and steel platform decks, situated near Essex, England. (e, g) Coastal transmission tower near Sabancuy, Mexico.

4.1.2 Site-scale accuracy assessment and cross-comparisons

We spatially matched the dataset of OOGPs generated in this work with the BSEE dataset based on the nearest neighbor distance. Then, we calculated the distance between each detection point and its corresponding BSEE reference point and performed a statistical analysis of the distance error. Table 4 presents the spatial distribution and distance error statistics of our OOGPs points and platform points in comparative products. Based on spatial analysis within a nearest neighbor distance of 10 m, 5180 points were matched with the corresponding validation data points. The number of sample points in the GoM and PG was significantly higher than that in other regions, at 1451 and 1397, respectively. Overall, OOGPs achieved a mean error of 0.35 m, median error of 0.05m, standard deviation error of 0.64m, maximum error of 3.29 m, and minimum error of 0 m. Among all regions, the GoM demonstrated the highest spatial consistency, with a mean error of 0.06 and a median error

https://doi.org/10.5194/essd-2026-63
Preprint. Discussion started: 4 February 2026

approximating 0 m. Its high accuracy is attributed to the type of platform and the large number of validation sample points in the GoM. In contrast, the GoT exhibited the highest distance error, likely because of the limited validation sample points. Notably, the type and design of platforms differ across varying offshore areas; therefore, the size of these offshore structures should be considered when validating their locations.

Table 4. Transposed error distance statistics (meter) for different regions.

Region	Mean	Median	Standard deviation	Maximum	Minimum	Points matched
PG	0.18	0.06	0.24	1.04	0.00	1451
CS	0.13	0.04	0.38	4.09	0.00	839
GoM	0.06	0.00	0.12	0.84	0.00	1397
GoG	0.61	0.03	1.11	4.38	0.00	423
GoT	0.95	0.16	1.48	6.33	0.00	626
NS	0.19	0.00	0.49	3.04	0.00	444
Total	0.35	0.05	0.64	3.29	0.00	5180

We further visually compared our OOGPs map product with the existing datasets from BSEE and OGIM platform for 2023 at the offshore basin scale (Fig. 9). The unmatched red points in Fig.9 (c) represent platforms removed before 2023. Since the absence of detailed removal dates in the OGIM dataset, such inactive platforms could not be excluded from the records, limiting its temporal accuracy. In contrast, our OOGPs dataset provides enhanced temporal resolution by focusing on actively present platforms. This enables clearer and more timely detection of platform distribution changes, especially in dynamic production areas where some OGIM platforms may have been removed but not updated in attribution. Spatially, our dataset offers broader and denser platform coverage in marginal seas and nearshore zones that are often underrepresented in existing products. As shown in panels (a–c) of Fig. 9, the OOGPs map shows more comprehensive distributions in key oil and gas regions such as the NGoM, GoG, and GoT. More detailed validation were described in Fig.S5 and Fig.S6 in the supplymentary material. Overall, the proposed OOGPs dataset holds significant international value by filling critical gaps in existing global offshore infrastructure inventories. Existing datasets, such as BSEE or OGIM, often suffer from low update frequencies, incomplete metadata, and inconsistent reporting standards. Our approach provides a unified, timely, and spatially detailed view of offshore platforms using time-series Sentinel-1 SAR imagery based on an adaptive detection framework. Beyond spatial and temporal completeness, the dataset also incorporates key platform attributes such as flaring activity, derived from long-term thermal anomaly detection. This attribute provides insights into operational status and potential environmental impact, which are often lacking in existing inventories.

The enhanced detail and reliability of the OOGPs dataset enables a wide range of applications, including: (1) global environmental monitoring, such as tracking emissions, identifying oil spill risks, and assessing marine ecosystem impacts; (2) maritime domain awareness, including vessel interaction analysis, infrastructure security, and illegal activity surveillance; (3) energy transition tracking, where timely and accurate data on fossil fuel infrastructure is critical for national decarbonization

https://doi.org/10.5194/essd-2026-63
Preprint. Discussion started: 4 February 2026

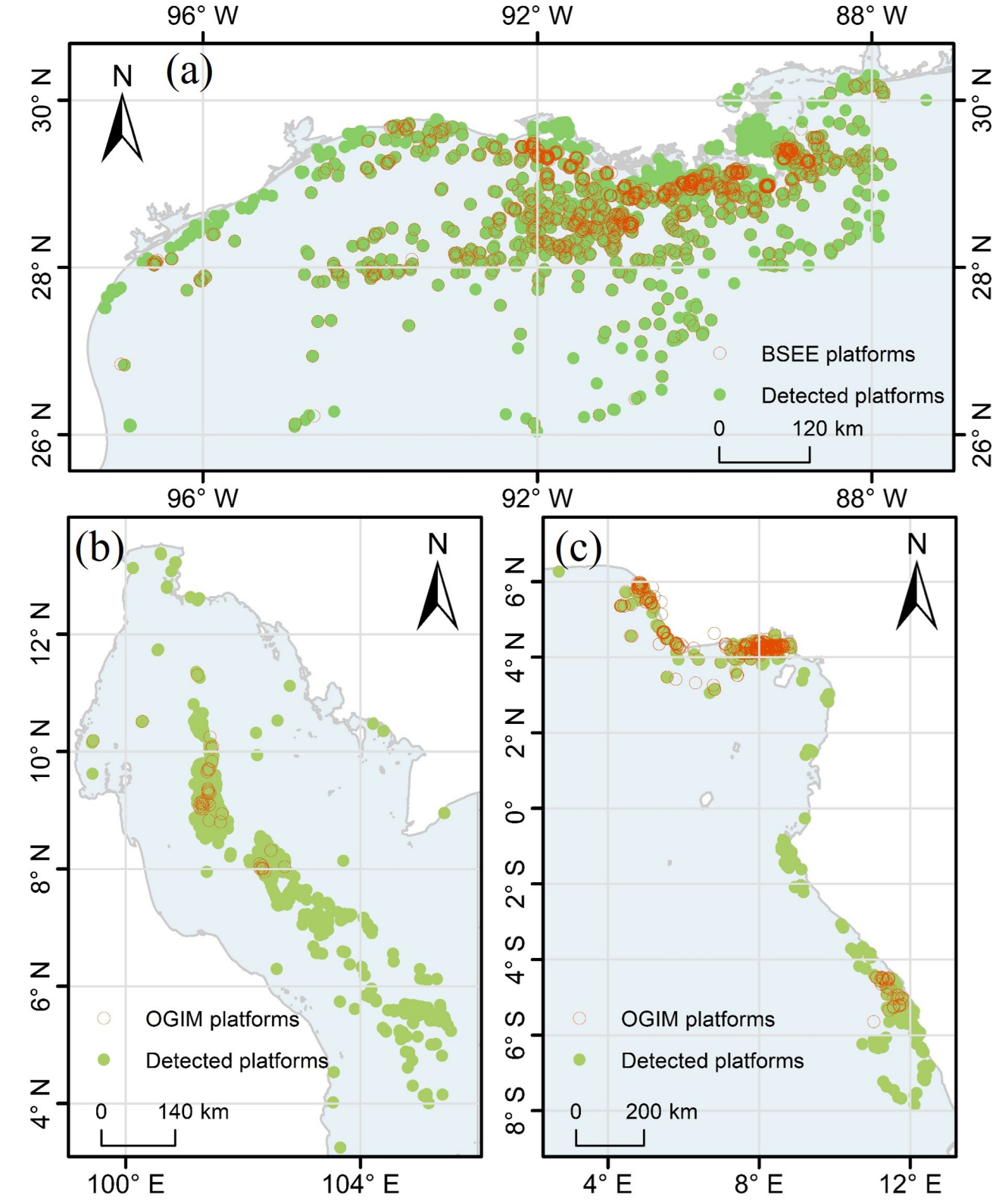

Figure 9. Comparison of the OOGPs map and BSEE or OGIM production in 2023. Green points represent OOGPs detected by Sentinel-1. The red circles indicate the referenced production. Panels (a), (b), and (c) indicate comparisons of the NoGM, GoT, and GoG, respectively.

https://doi.org/10.5194/essd-2026-63
Preprint. Discussion started: 4 February 2026

planning and offshore wind site assessments. By offering a more comprehensive inventory across various regions, this dataset contributes to improved global transparency, data interoperability, and decision-making in offshore energy management and remote sensing applications.

4.2 Temporal patterns of OOGPs from 2017 to 2023

An open-source OOGPs dataset with detailed spatial and temporal information plays an important role in understanding temporal patterns in offshore oil and gas infrastructure and attributing satellite-observed GHG emissions to upstream fossil fuel operations. In particular, the inclusion of offshore GFs labels enables assessment of the prevalence of unlit flaring, improving the attribution of satellite-detected methane plumes to specific sources.

We acquired approximately 5,358 existing OOGPs. Its records including point-based OOGP locations, facility areas, EEZs, and GFs activity labels. Among all records, the GoM accounted for the largest share, nearly 30% of total entries in 2023, followed by the PG and CS. The GoG holds the smaller share, around 8.6%, but still displays notable flare activity. This reveals the environmental relevance of even smaller offshore regions due to the lack of investment or availability of gas infrastructure.

As illustrated in Fig. 10 (a), the temporal analysis reveals trends in the six selected regions from 2017 to 2023. The GoM showed a gradual decrease in the number of detected platforms, primarily driven by the decommissioning of aging infrastructure, reduced investment in new exploration, and broader shifts toward cleaner energy policies. Despite this decrease, the number of GoM platforms with GF remained stable or slightly increased, suggesting more intensive production activities at remaining facilities, as well as the persistence of legacy infrastructure that lacks sufficient gas capture or reinjection systems. The mismatch between platform decommissioning and flaring mitigation efforts highlights ongoing infrastructure and policy challenges in managing associated emissions. In contrast, the PG exhibited a gradual increase in both the number of OOGPs and those with GFs, which may reflect the expansion of production capacity, the deployment of new platforms, or operational inefficiencies associated with maintenance. The CS and GoT show smaller but similar trends, with moderate year-to-year fluctuations likely driven by project-level cycles or maintenance schedules.

The pie charts in Fig. 10 (b–h) present annual distributions of OOGPs across the six offshore basins between 2017 and 2023. The GoM consistently ranked as the leading area in terms of OOGPs count, although its dominance gradually declined from 37.4% in 2017 to 29.7% in 2023. Meanwhile, the PG's share gradually increased from 20.4% in 2017 to 26.8% in 2023, confirming regional growth.

To further examine national dynamics, Fig. 11 provides the annual OOGPs detection counts and associated flare activity for individual countries. The United States remained the leader in offshore oil and gas infrastructure among all countries in this study, despite a slight decline year-over-year. In contrast, Saudi Arabia and the UAE experienced a steady rise in OOGP detections, reflecting large-scale field development and offshore investment. This makes them the second-largest contributors after the United States (Kaiser, 2022; Chen et al., 2024). Other key countries, including Mexico, Iran, Malaysia, Netherlands, and Nigeria, maintained relatively stable detection counts, each with over 100 platforms annually. Notably, Azerbaijan also exhibited a relatively high number of detected OOGPs despite its more limited offshore area. This can be attributed to the unique structural configuration of its offshore facilities, particularly the Oil Rocks (Neft Daşları) complex in the CS (See example in

https://doi.org/10.5194/essd-2026-63
Preprint. Discussion started: 4 February 2026

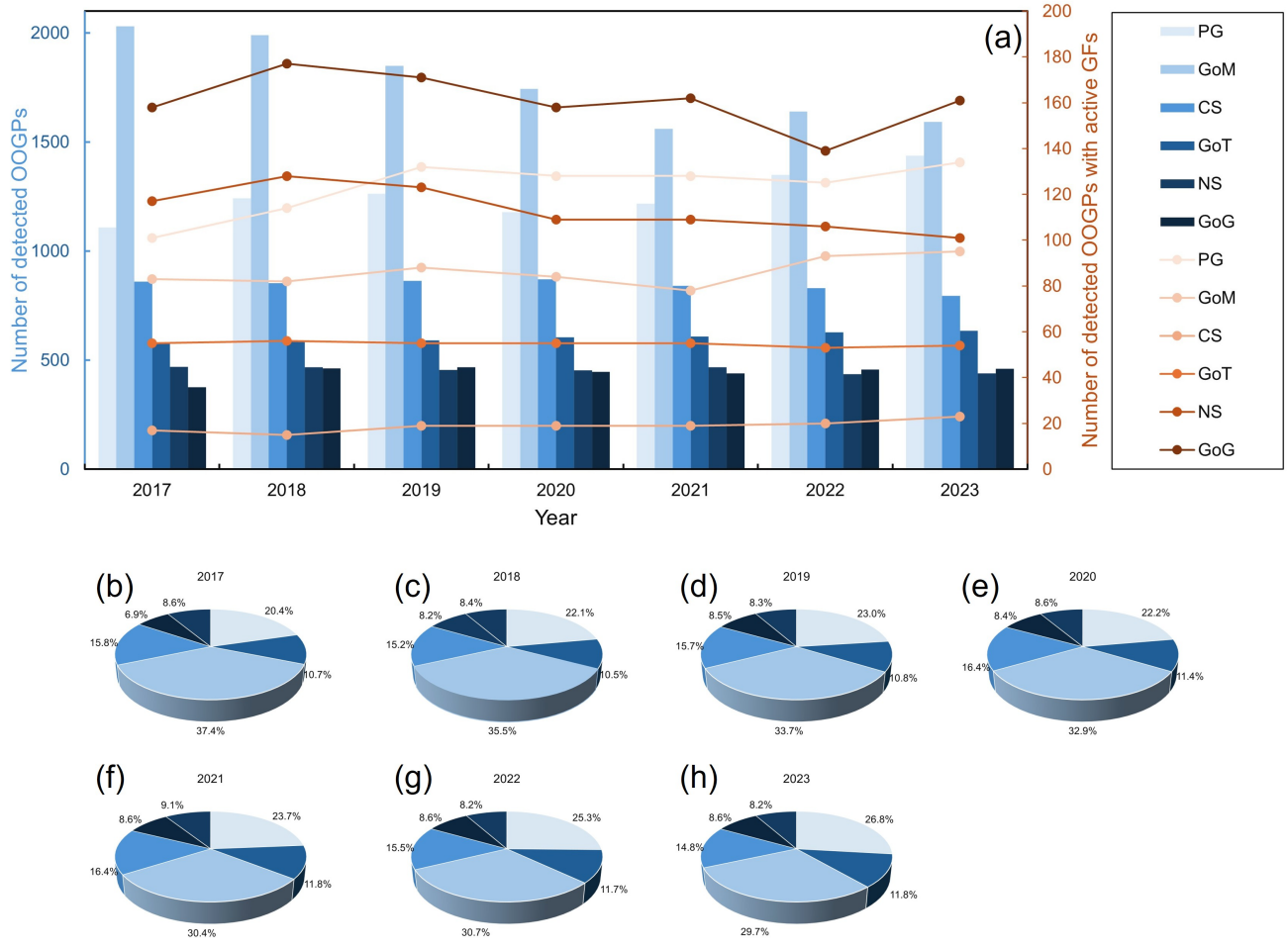

Figure 10. (a) Temporal evolution of detected OOGPs and numbe of OOGPs with active gas flarings (GFs) in select regions, (b)-(h) the proportion of each offshore basin based on available data from 2017 to 2023.

Fig. 2 (i)). Unlike traditional standalone platforms, Oil Rocks consists of a network of numerous small interconnected production units and walkways constructed over shallow waters. These discrete elements are often identified as multiple independent platforms from satellite imagery, leading to a higher overall detection count in Azerbaijan. Similarly, Thailand maintained a dense distribution of small-scale offshore infrastructure in the GoT. These eleven countries collectively accounted for approximately 90% of all OOGPs detected in the study areas, reflecting a clear spatial concentration of OOGPs.

In summary, this multi-year dataset offers insights into operational shifts in offshore fossil fuel development. It reveals regional changes including the decline of infrastructure and steady GFs in the GoM; platform expansion and increasing GFs activity in the PG; and flare-associated intensity variations in the GoG. It also highlights national-level strategies, with countries like the United States and Saudi Arabia pursuing distinct trajectories in offshore energy development. These insights are critical

https://doi.org/10.5194/essd-2026-63
Preprint. Discussion started: 4 February 2026

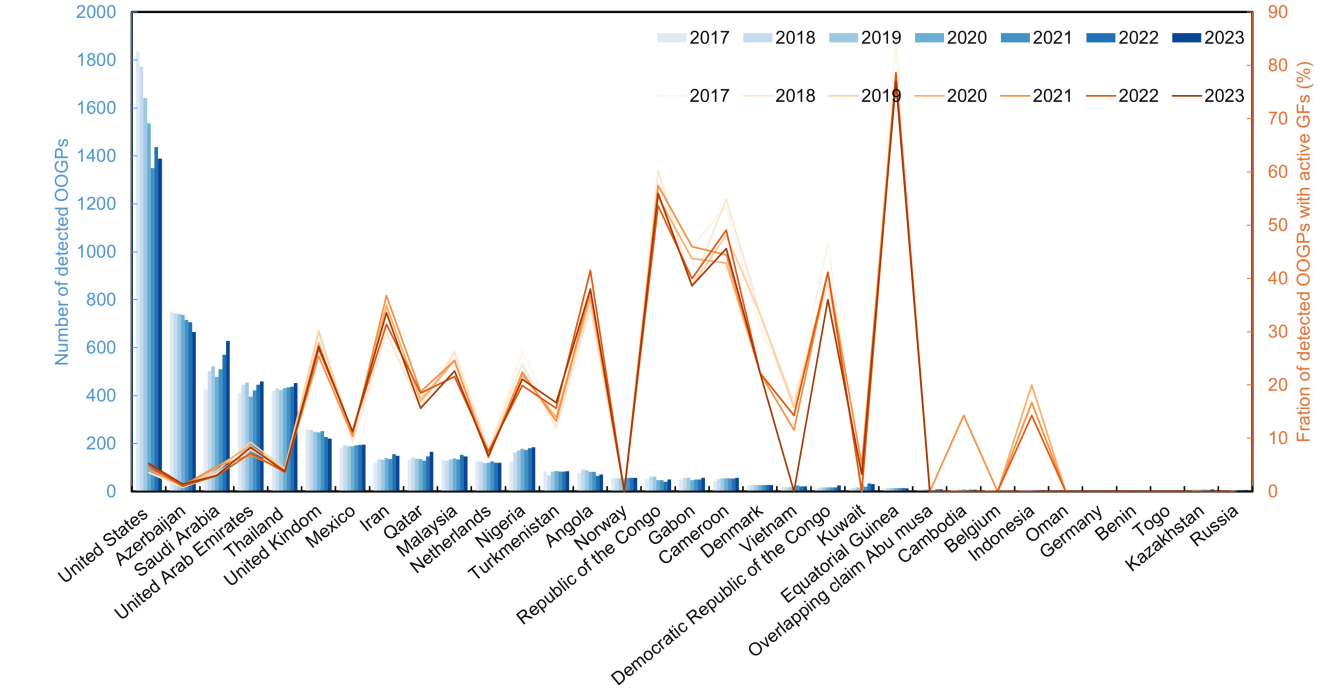

Figure 11. National temporal evolution of OOGPs as detected in this study, and the fraction of OOGPs with active gas flarings (GFs) as indicated by Sentinel-2 data from 2017 to 2023.

4.3 Spatial distribution patterns of OOGPs in different EEZs

Figure 12 illustrates the distinct spatial distribution patterns of OOGPs detected in various EEZs of the selected ROIs. The green points represent existing platforms until 2023 and the red points represent platforms removed from 2017 to 2023 in the corresponding EEZ region. OOGPs are highly clustered in major oil-producing regions, with varying densities and removal histories. The United States has the most OOGPs in all selected EEZs. The GoM, GoT, and PG EEZs, such as the United States, Saudi Arabia, UAE, and Thailand, exhibit the highest density characteristics, with clear spatial linear patterns and small-scale cluster patterns along structural basin belts, whereas the distribution of platforms in the NS is relatively widespread. This indicates that the distribution of oil and gas fields is controlled by regional tectonic and geological conditions, with hydrocarbon resources mainly concentrated in structural highs and fault zones within sedimentary basins. The significant number of platforms removed in the NGoM, NS, and GoT regions can be attributed to the extensive presence of active movable

https://doi.org/10.5194/essd-2026-63
Preprint. Discussion started: 4 February 2026

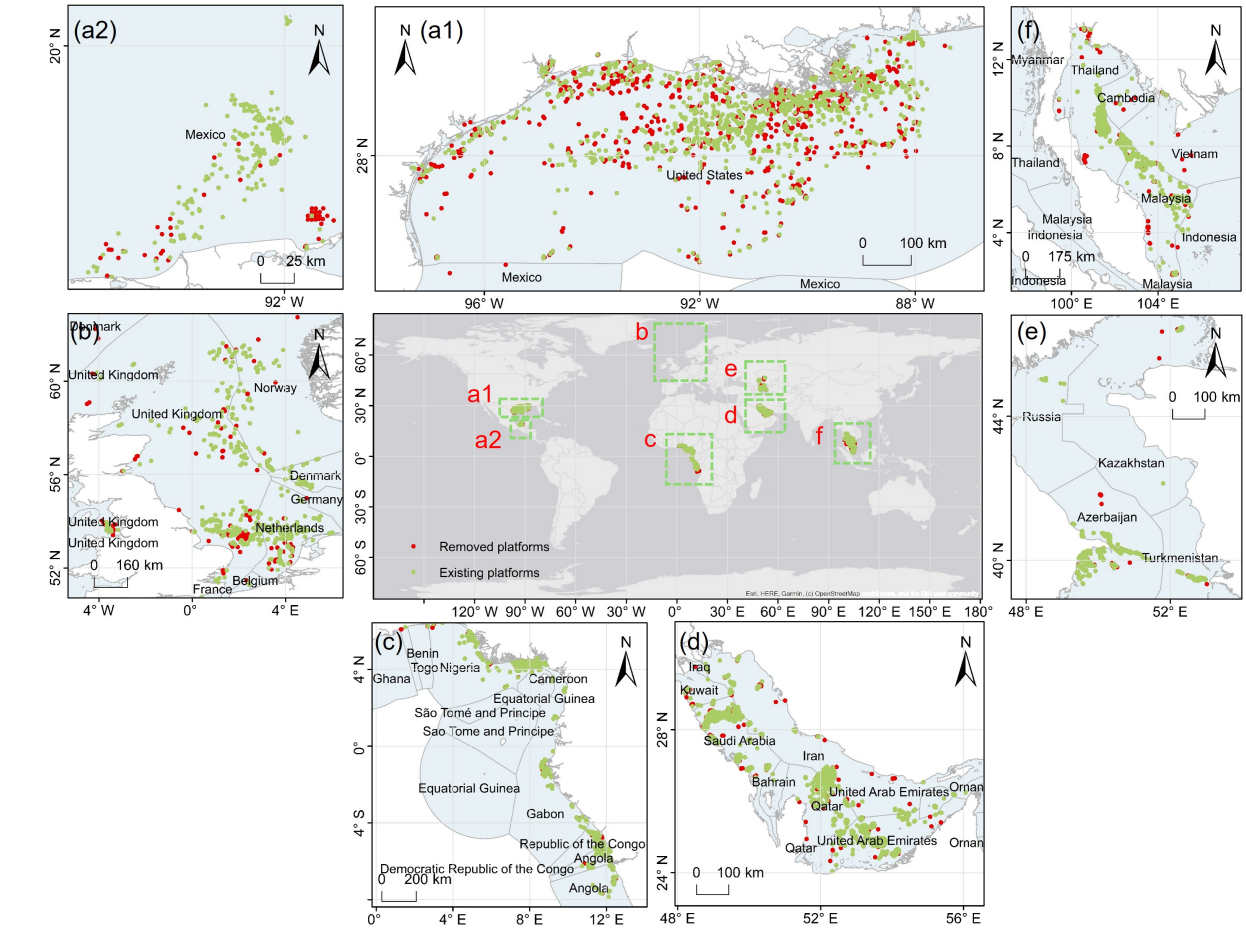

Figure 12. Spatial distribution of OOGPs detected in select regions based on available data from 2017 to 2023. Zoom-in insets of the NGoM, SGOM, NS, GoG, Persian Gulf, and GoT. The colours of OOGPs represent their status (green = existing and red = removed).

4.4 Discussion

This study aims to improve the automation and timeliness of offshore platform detection, thereby better supplementing existing government reporting data; however, certain limitations and uncertainties remain in this study. The detection of platforms near the coastline is constrained by blurred shorelines, rocky coasts, and intertidal mudflats. To mitigate these effects, a 500 m buffer zone from the coastline was applied, and all objects within this zone were manually checked; objects located within 500

https://doi.org/10.5194/essd-2026-63
Preprint. Discussion started: 4 February 2026

meters of the coast were excluded from detection. Platforms close to the shore also tend to be smaller in size, which further complicates detection.

Detection of platforms using Sentinel-1 SAR imagery is additionally limited by the spatial resolution of the data. Platforms smaller than approximately 5×20 m are difficult to detect, and smaller platforms are also affected by sea surface conditions such as wind speed, ocean clutter, and nearshore sediment content, as well as the radar incidence angle. These factors make it challenging to distinguish small platforms from a rough sea surface, which may lead to underestimation of platform numbers in regions with high platform density, such as the GoM and the PG.

In future research, the fusion of multi-source remote sensing data is expected to improve the completeness and accuracy of the platform dataset, particularly for small or nearshore platforms.

5 Conclusions

This study produced a vectorized OOGPs dataset that provides OOGPs locations and status in six offshore basins: the GoM, NS, GoG, GoT, PG, and CS. We present a framework for OOGPs detection based on an adaptive threshold model and morphological operations using time-series Sentinel-1 SAR images and Sentinel-2 MSI images from 2017 to 2023. The effectiveness and robustness of the proposed framework were demonstrated by creating a comprehensive validation dataset and assessing the accuracy between our detected and validation datasets. Our method can effectively remove different types of false positive targets, such as OWTs, ships, and signal noise.

As of 2023, 5,358 OOGPs have been identified with 1,593, 1,437, 440, 794, 460, and 634 in the GoM, PG, NS, CS, GoG, and GoT, respectively. These six basin regions have distinct numbers of OOGPs, with the GoM and PG leading in terms of deployment. Most OOGPs exhibit regular linear or clustered spatial distributions, revealing the geographical concentration and regional variation in offshore energy infrastructure. The attribute information of this updated and completed dataset meets the critical geospatial data needs to support offshore environmental monitoring, facility-scale pollutant gas emission tracking, assessment and mitigation.

The GoM has witnessed a clear trend of decommissioning OOGPs, indicating its long history of exploration and development. However, the installation of OOGPs has exhibited a remarkable exponential growth trend in PG from 2017 to 2023. Despite having the fewest or second-fewest platforms between 2017 and 2023, the GoG exhibited the highest level of GF activity. These variations provide valuable insights into regional development trajectories and environmental risks associated with offshore infrastructure.

The validation and assessment results highlight the effectiveness of our detection method with high precision and recall rates. The OOGPs dataset achieved an overall accuracy of 0.99 and a mean error distance of 0.35 m. In addition, compared with the OGIM dataset, our results establish higher coverage detections with detailed location, country, EEZs, area, and GFs status over a long period.

https://doi.org/10.5194/essd-2026-63
Preprint. Discussion started: 4 February 2026

6 Data availability

The OOGPs data is available from https://doi.org/10.5281/zenodo.18350974 (Si et al., 2026) in an open-access vector file format. All records were produced and tested using GEE, Python, and ArcGIS 10.8. It provides the spatiotemporal distribution and statue of OOGPs in the GoM, NS, GoG, GoT, PG, and CS from 2017 to 2023.

Appendix A: Acronyms and Abbreviations

Abbreviation	Definition	Abbreviation	Definition
BSEE	Bureau of Safety and Environmental Enforcement	CS	Caspian Sea
CH_4	Methane	CPP	Central Processing Platform
DEM	Digital Elevation Model	EC	European Commission
EEZ	Exclusive Economic Zone	ESA	European Space Agency
FPSO	Floating production, storage and offloading	GEE	Google Earth Engine
GF	Gas Flaring	GHG	Greenhouse Gas
GoG	Gulf of Guinea	GoM	Gulf of Mexico
GoT	Gulf of Thailand	GRD	Ground Range Detected
HH	Horizontal transmit/Horizontal receive	HTA	High-Temperature Anomaly
HV	Horizontal transmit/Vertical receive	IW	Interferometric Wide
MARS	Methane Alert and Response System	MK	Mann–Kendall
MODU	Moveable Offshore Drilling Unit	MSI	MultiSpectral Instrument
NGoM	Northern Gulf of Mexico	NRT	Near Real-Time
NS	North Sea	OF	Occurrence Frequency
OESNS	Offshore Energy Structure in the North Sea		
OGIM	Oil and Gas Infrastructure Mapping	OOGP	Offshore oil and gas platform
OWF	Offshore Wind Farm	OWT	Offshore Wind Turbine
PG	Persian Gulf	RGB	Red, Green, Blue
ROI	Regions of interest	SAR	Synthetic Aperture Radar
SGoM	Southern Gulf of Mexico	SWIR	Shortwave Infrared
TAI	Thermal Anomaly Index	TOA	Top-Of-Atmosphere
UAE	United Arab Emirates	UNEP	United Nations Environment Program
VV	Vertical transmit/Vertical receive	VNIR	Visible and Near-Infrared
VH	Vertical transmit/Horizontal receive		

https://doi.org/10.5194/essd-2026-63
Preprint. Discussion started: 4 February 2026

Open Access Earth System Science Data Discussions

Competing interests. The contact author has declared that none of the authors has any competing interests.

Disclaimer. Publisher's note: Copernicus Publications remains neutral with regard to jurisdictional claims in published maps and institutional affiliations.

Acknowledgements. This research was supported by the China Scholarship Council (Grant number:202306220072) and funded by UNEP's International Methane Emissions Observatory (IMEO). The authors thank the Copernicus Programme of the European Space Agency for the free provision of Sentinel-1 and Sentinel-2 data, and the Google Earth Engine platform for enabling efficient data preprocessing and access. We also express our sincere appreciation to all data providers of BSEE, OGIM, NOAA, OESNS and FIRMS production for their sharing.

https://doi.org/10.5194/essd-2026-63
Preprint. Discussion started: 4 February 2026

Open Access Earth System Science Data Discussions

References

Annex I: Glossary, in: Global Warming of 1.5°C: IPCC Special Report on Impacts of Global Warming of 1.5°C above Pre-industrial Levels in Context of Strengthening Response to Climate Change, Sustainable Development, and Efforts to Eradicate Poverty, edited by Intergovernmental Panel on Climate Change (IPCC), pp. 541–562, Cambridge University Press, Cambridge, ISBN 978-1-00-915795-7, https://doi.org/10.1017/9781009157940.008, 2022.

Allen, M., Mustafa, B., and Shukla, P.: GLOBAL WARMING OF 1.5 °C - an IPCC special report on the impacts of global warming of 1.5 °C above pre-industrial levels and related global greenhouse gas emission pathways, in the context of strengthening the global response to the threat of climate change, sustainable development, and efforts to eradicate poverty, 2018.

Alvarez, R. A., Zavala-Araiza, D., Lyon, D. R., Allen, D. T., Barkley, Z. R., Brandt, A. R., Davis, K. J., Herndon, S. C., Jacob, D. J., Karion, A., Kort, E. A., Lamb, B. K., Lauvaux, T., Maasakkers, J. D., Marchese, A. J., Omara, M., Pacala, S. W., Peischl, J., Robinson, A. L., Shepson, P. B., Sweeney, C., Townsend-Small, A., Wofsy, S. C., and Hamburg, S. P.: Assessment of methane emissions from the U.S. oil and gas supply chain, Science, 361, 186–188, https://doi.org/10.1126/science.aar7204, publisher: American Association for the Advancement of Science, 2018.

Anifowose, B., Lawler, D. M., van der Horst, D., and Chapman, L.: A systematic quality assessment of Environmental Impact Statements in the oil and gas industry, Science of The Total Environment, 572, 570–585, https://doi.org/10.1016/j.scitotenv.2016.07.083, 2016.

Bernstein, B. B.: Evaluating alternatives for decommissioning California's offshore oil and gas platforms, Integrated Environmental Assessment and Management, 11, 537–541, https://doi.org/10.1002/ieam.1657, 2015.

Cantle, P. and Bernstein, B.: Air emissions associated with decommissioning California's offshore oil and gas platforms, Integrated Environmental Assessment and Management, 11, 564–571, https://doi.org/10.1002/ieam.1653, _eprint: https://onlinelibrary.wiley.com/doi/pdf/10.1002/ieam.1653, 2015.

Casadio, S., Arino, O., and Minchella, A.: Use of ATSR and SAR measurements for the monitoring and characterisation of night-time gas flaring from off-shore platforms: The North Sea test case, Remote Sensing of Environment, 123, 175–186, https://doi.org/10.1016/j.rse.2012.03.021, 2012.

Charfeddine, L. and Barkat, K.: Short- and long-run asymmetric effect of oil prices and oil and gas revenues on the real GDP and economic diversification in oil-dependent economy, Energy Economics, 86, 104 680, https://doi.org/10.1016/j.eneco.2020.104680, 2020.

Chen, X., Wang, Z.-q., Li, C.-x., Gao, F., and Wei, Q.: Characteristics of Global Offshore Oil and Gas Development, https://doi.org/10.1007/978-981-97-0475-0_87, 2024.

Ekins, P., Vanner, R., and Firebrace, J.: Zero emissions of oil in water from offshore oil and gas installations: economic and environmental implications, Journal of Cleaner Production, 15, 1302–1315, https://doi.org/10.1016/j.jclepro.2006.07.014, 2007.

Elvidge, C., Zhizhin, M., Baugh, K., Hsu, F.-C., and Ghosh, T.: Methods for Global Survey of Natural Gas Flaring from Visible Infrared Imaging Radiometer Suite Data, Energies, 9, 14, https://doi.org/10.3390/en9010014, 2015.

Elvidge, C. D., Zhizhin, M., Baugh, K., Hsu, F.-C., and Ghosh, T.: Methods for Global Survey of Natural Gas Flaring from Visible Infrared Imaging Radiometer Suite Data, Energies, 9, 14, https://doi.org/10.3390/en9010014, number: 1 Publisher: Multidisciplinary Digital Publishing Institute, 2016a.

Elvidge, C. D., Zhizhin, M., Baugh, K., Hsu, F.-C., and Ghosh, T.: Methods for Global Survey of Natural Gas Flaring from Visible Infrared Imaging Radiometer Suite Data, Energies, 9, 14, https://doi.org/10.3390/en9010014, number: 1 Publisher: Multidisciplinary Digital Publishing Institute, 2016b.

https://doi.org/10.5194/essd-2026-63
Preprint. Discussion started: 4 February 2026

Falqueto, L. E., Sá, J. A. S., Paes, R. L., and Passaro, A.: Oil Rig Recognition Using Convolutional Neural Network on Sentinel-1 SAR Images, IEEE Geoscience and Remote Sensing Letters, 16, 1329–1333, https://doi.org/10.1109/LGRS.2019.2894845, conference Name: IEEE Geoscience and Remote Sensing Letters, 2019.

Faruolo, M., Genzano, N., Marchese, F., and Pergola, N.: Multi-Temporal Satellite Investigation of gas Flaring in Iraq and Iran: The DAFI Porting on Collection 2 Landsat 8/9 and Sentinel 2A/B, Sensors, 23, 5734, https://doi.org/10.3390/s23125734, publisher: Multidisciplinary Digital Publishing Institute, 2023.

Hamed, K. H.: Trend detection in hydrologic data: The Mann–Kendall trend test under the scaling hypothesis, Journal of Hydrology, 349, 350–363, https://doi.org/10.1016/j.jhydrol.2007.11.009, 2008.

Henrion, M., Bernstein, B., and Swamy, S.: A multi-attribute decision analysis for decommissioning offshore oil and gas platforms, Integrated Environmental Assessment and Management, 11, 594–609, https://doi.org/10.1002/ieam.1693, _eprint: https://onlinelibrary.wiley.com/doi/pdf/10.1002/ieam.1693, 2015.

Hoeser, T., Feuerstein, S., and Kuenzer, C.: DeepOWT: a global offshore wind turbine data set derived with deep learning from Sentinel-1 data, Earth System Science Data, 14, 4251–4270, https://doi.org/10.5194/essd-14-4251-2022, publisher: Copernicus GmbH, 2022.

Hunt, J. D., Nascimento, A., Nascimento, N., Vieira, L. W., and Romero, O. J.: Possible pathways for oil and gas companies in a sustainable future: From the perspective of a hydrogen economy, Renewable and Sustainable Energy Reviews, 160, 112 291, https://doi.org/10.1016/j.rser.2022.112291, 2022.

IEA: World Energy Outlook 2024, https://www.iea.org/reports/world-energy-outlook-2024, licence: CC BY 4.0 (report); CC BY NC SA 4.0 (Annex A), 2024.

Irakulis-Loitxate, I., Gorroño, J., Zavala-Araiza, D., and Guanter, L.: Satellites Detect a Methane Ultra-emission Event from an Offshore Platform in the Gulf of Mexico, Environmental Science & Technology Letters, 9, 520–525, https://doi.org/10.1021/acs.estlett.2c00225, publisher: American Chemical Society, 2022.

Jiasheng, W., Yongxue, L. I. U., Manchun, L. I., Kang, Y., and Liang, C.: Drilling platform detection based on ENVISAT ASAR remote sensing dataA case of southeastern Vietnam offshore area, GEOGRAPHICAL RESEARCH, 32, 2143–2152, https://doi.org/10.11821/dlyj201311015, number: 11, 2013.

Kaiser, M. J.: Offshore oil and gas records circa 2020, Taylor & Francis, https://www.tandfonline.com/doi/abs/10.1080/17445302.2020.1827633, publisher: Taylor & Francis, 2022.

Kendall, M.: Rank correlation methods, Rank correlation methods, Griffin, Oxford, England, 1948.

Lee, J.: The regional economic impact of oil and gas extraction in Texas, Energy Policy, 87, 60–71, https://doi.org/10.1016/j.enpol.2015.08.032, 2015.

Liu, Y., Sun, C., Yang, Y., Zhou, M., Zhan, W., and Cheng, W.: Automatic extraction of offshore platforms using time-series Landsat-8 Operational Land Imager data, Remote Sensing of Environment, 175, 73–91, https://doi.org/10.1016/j.rse.2015.12.047, 2016.

Liu, Y., Pu, Y., Hu, X., Dong, Y., Wu, W., Hu, C., Zhang, Y., and Wang, S.: Global declines of offshore gas flaring inadequate to meet the 2030 goal, Nature Sustainability, 6, 1095–1102, https://doi.org/10.1038/s41893-023-01125-5, number: 9 Publisher: Nature Publishing Group, 2023.

Mann, H. B.: Nonparametric Tests Against Trend, Econometrica, 13, 245–259, https://doi.org/10.2307/1907187, publisher: [Wiley, Econometric Society], 1945.

Martins, M. C. I., Carter, M. I., Rouse, S., and Russell, D. J.: Offshore energy structures in the North Sea: Past, present and future, Marine Policy, 152, 105 629, https://doi.org/10.1016/j.marpol.2023.105629, 2023.

https://doi.org/10.5194/essd-2026-63
Preprint. Discussion started: 4 February 2026

Nguyen, T.-V., Tock, L., Breuhaus, P., Maréchal, F., and Elmegaard, B.: CO2-mitigation options for the offshore oil and gas sector, Applied Energy, 161, 673–694, https://doi.org/10.1016/j.apenergy.2015.09.088, 2016.

Omara, M., Gautam, R., O'Brien, M. A., Himmelberger, A., Franco, A., Meisenhelder, K., Hauser, G., Lyon, D. R., Chulakadabba, A., Miller, C. C., Franklin, J., Wofsy, S. C., and Hamburg, S. P.: Developing a spatially explicit global oil and gas infrastructure database for characterizing methane emission sources at high resolution, Earth System Science Data, 15, 3761–3790, https://doi.org/10.5194/essd-15-3761-2023, publisher: Copernicus GmbH, 2023.

Peng, C., Wang, J., and Li, D.: Oil platform investigation by multi-temporal SAR remote sensing image, in: SAR Image Analysis, Modeling, and Techniques XI, vol. 8179, pp. 257–264, SPIE, https://doi.org/10.1117/12.897937, 2011.

Ronconi, R. A., Allard, K. A., and Taylor, P. D.: Bird interactions with offshore oil and gas platforms: Review of impacts and monitoring techniques, Journal of Environmental Management, 147, 34–45, https://doi.org/10.1016/j.jenvman.2014.07.031, 2015.

Si, L., Zhou, S., Irakulis-Loitxate, I., Roger, J., and Guanter, L.: The Offshore Oil and Gas Platforms (OOGPs) dataset based on satellite data spanning 2017 to 2023, Zenodo [data set], https://doi.org/10.5281/zenodo.18350974, 2026.

Spanier, R. and Kuenzer, C.: Marine Infrastructure Detection with Satellite Data—A Review, Remote Sensing, 16, 1675, https://doi.org/10.3390/rs16101675, 2024.

Tan, Y., Li, H. X., Cheng, J. C. P., Wang, J., Jiang, B., Song, Y., and Wang, X.: Cost and environmental impact estimation methodology and potential impact factors in offshore oil and gas platform decommissioning: A review, Environmental Impact Assessment Review, 87, 106 536, https://doi.org/10.1016/j.eiar.2020.106536, 2021.

Wang, Z., Li, S., Jin, Z., Li, Z., Liu, Q., and Zhang, K.: Oil and gas pathway to net-zero: Review and outlook, Energy Strategy Reviews, 45, 101 048, https://doi.org/10.1016/j.esr.2022.101048, 2023.

Wong, B. A., Thomas, C., and Halpin, P.: Automating offshore infrastructure extractions using synthetic aperture radar & Google Earth Engine, Remote Sensing of Environment, 233, 111 412, https://doi.org/10.1016/j.rse.2019.111412, 2019.

Zhang, T., Tian, B., Sengupta, D., Zhang, L., and Si, Y.: Global offshore wind turbine dataset, Scientific Data, 8, 191, https://doi.org/10.1038/s41597-021-00982-z, publisher: Nature Publishing Group, 2021.

Zhao, S., Sun, C., Wang, H., and Cheng, W.: Extraction and monitoring of offshore oil and gas platforms based on Landsat imagery, Trop. Geogr, 37, 112–119, 2017.

Zhu, H., Jia, G., Zhang, Q., Zhang, S., Lin, X., and Shuai, Y.: Detecting Offshore Drilling Rigs with Multitemporal NDWI: A Case Study in the Caspian Sea, Remote Sensing, 13, 1576, https://doi.org/10.3390/rs13081576, number: 8 Publisher: Multidisciplinary Digital Publishing Institute, 2021.